Journal of Solid State Chemistry 184 (2011) 2580–2587

Contents lists available at ScienceDirect

Journal of Solid State Chemistry

journal homepage: www.elsevier.com/locate/jssc

Structural and magnetic properties of $Nd_{18}Li_8Co_{4-x}Fe_xO_{39-y}$ and $Nd_{18}Li_8Co_{4-x}Ti_xO_{39-y}$

Peter D. Battle [a,*], Siân E. Dutton [a], Fernande Grandjean [b], Gary J. Long [c], Nirawat Thammajak [a], Sirikarn Wisetsuwannaphum [a]

[a] Inorganic Chemistry Laboratory, Department of Chemistry, University of Oxford, South Parks Road, Oxford, OX1 3QR, UK
[b] Faculty of Sciences, University of Liège, B-4000 Sart-Tilman, Belgium
[c] Department of Chemistry, Missouri University of Science and Technology, University of Missouri, Rolla, Missouri 65409-0010, USA

ARTICLE INFO

Article history:
Received 6 May 2011
Received in revised form
30 June 2011
Accepted 6 July 2011
Available online 28 July 2011

Keywords:
Mixed-metal oxides
Neutron diffraction
Antiferromagnetism
Spin glass

ABSTRACT

$Nd_{18}Li_8Co_3FeO_{39-y}$, $Nd_{18}Li_8CoFe_3O_{39-y}$ and $Nd_{18}Li_8Co_3TiO_{39-y}$ have been synthesised and characterised by neutron powder diffraction, magnetometry and Mössbauer spectroscopy. Their cubic structure ($Pm\bar{3}n$, $a \sim 11.9$ Å) is based on intersecting $<1\,1\,1>$ chains comprised of alternating octahedral and trigonal-prismatic coordination sites. These chains lie within hexagonal-prismatic cavities formed by a Nd–O framework. Each compound has an incomplete oxide sublattice ($y \sim 1$), with vacancies located around the octahedral sites that lie at the points of chain intersection. These sites are fully occupied by a disordered arrangement of transition-metal cations but only 75% of the remaining octahedral sites are occupied. The trigonal-prismatic sites are fully occupied by lithium except in the case of $Nd_{18}Li_8CoFe_3O_{39-y}$ where some iron is present. Antiferromagnetic interactions are present on the Nd sublattice in each composition, but a spin glass forms below 5 K when a high concentration of spins is also present on the octahedral sites.

1. Introduction

The crystal structure drawn in Fig. 1 was first described in detail in an account [1] of the synthesis and characterisation of $Ln_{18}Li_8Rh_5O_{39}$ (Ln=La, Pr). The cubic unit cell (space group $Pm\bar{3}n$) was found to contain $<1\,1\,1>$ chains of alternating RhO_6 octahedra and LiO_6 prisms, with adjacent polyhedra being linked by face-sharing. The chains intersect at the origin and the body centre of the unit cell, and each chain segment occupies a hexagonal-prismatic cavity within the Ln–O framework. The octahedra are not all equivalent; those centred on the 2*a* sites at (0 0 0) and (½ ½ ½) are significantly smaller than those centred on the 8*e* sites at (¼ ¼ ¼) and equivalent positions. The multiplicity ratio of the two octahedral sites is thus 1:4, as is the ratio of Rh^{4+}: Rh^{3+} cations in these oxides. It was therefore proposed that these compounds were the first to exhibit an ordered arrangement of Rh^{4+} and Rh^{3+} in a mixed-valence oxide. It has subsequently been shown that this structure type can accommodate a wide range of chemical compositions [2–6]; rhodium may be substituted by various combinations of titanium, manganese, iron, cobalt or ruthenium, with Ln=lanthanum, praseodymium or neodymium. The choice of lanthanide cation controls, to some extent, the range of transition-metal cations that can be accommodated in the octahedral sites. This has been ascribed to the need to match the size of the *d*-block cation to the size of the cavity created by the Ln–O framework. It has also been shown that the magnetic behaviour of the oxides at low temperatures depends on the choice of Ln; compounds containing paramagnetic Nd^{3+} or Pr^{3+} often behave as spin glasses, whereas those containing diamagnetic La^{3+} do not.

$La_{18}Li_8Fe_5O_{39}$ and $Nd_{18}Li_8Fe_5O_{39}$ are among the compositions to have been studied to date. However, our attempts to prepare the cobalt analogues were unsuccessful. In the case of the neodymium–cobalt system, a $LiCoO_2$ impurity was identified in the X-ray diffraction pattern of the reaction product and we were subsequently able to prepare a monophasic sample of the cobalt-deficient composition $Nd_{18}Li_8Co_4O_{39}$. A study of this compound by neutron diffraction [2] showed that the small 2*a* site is fully occupied and that the cation deficiency is accommodated by vacancies on the 8*e* site alone. The analysis of neutron powder diffraction data did not reveal any oxygen deficiency in this compound and thus led to the conclusion that all the occupied octahedra contain Co^{4+} cations. It was argued that the high concentration of electropositive Nd^{3+} and Li^+ cations would stabilise this unusual oxidation state. Consideration of the bond lengths in $Nd_{18}Li_8Co_4O_{39}$ and other compositions [3] in this structural family generated the hypothesis that the Ln–O

* Corresponding author. Fax: +44 1865 272690.
E-mail address: peter.battle@chem.ox.ac.uk (P.D. Battle).

0022-4596/$ - see front matter © 2011 Elsevier Inc. All rights reserved.
doi:10.1016/j.jssc.2011.07.020

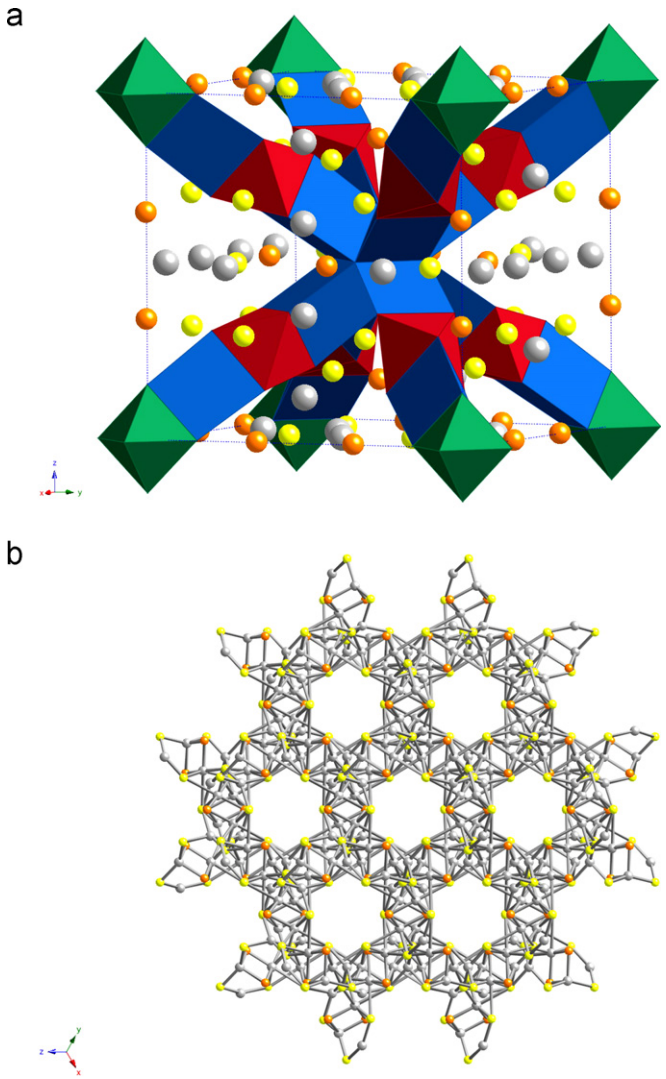

Fig. 1. (a) Polyhedral representation of the cubic (space group $Pm\bar{3}n$) structure of $La_{18}Li_8Rh_5O_{39}$; LiO_6 trigonal prisms are blue (16*i* site), RhO_6 octahedra are green (2*a*) and red (8*e*), grey circles represent oxygen (O2 and O3), yellow circles La1 and orange circles La2. (b) The La–O2–O3 framework viewed along $<1\,1\,1>$; the polyhedral chains run through the channels. (For interpretation of the references to color in this figure legend, the reader is referred to the web version of this article.)

framework exerts a significant chemical pressure on the network of polyhedra, thus providing another justification for the stability of the high oxidation state. Magnetic measurements suggested that the Co^{4+} cations are in a low-spin state, as would be expected in a high-pressure environment. The observation [3] by Mössbauer spectroscopy of low-spin Fe^{4+} in the solid solution $Nd_{18}Li_8Fe_{5-x}M_xO_{39}$ (M=Co, Mn) is consistent with the hypothesis that the *Ln*–O framework can exert a high chemical pressure in these systems.

We have now carried out further studies in an attempt to establish the circumstances under which cation-deficient members of this family can be formed, and we describe below the synthesis and characterisation of $Nd_{18}Li_8Co_{4-x}Fe_xO_{39-y}$ and $Nd_{18}Li_8Co_{4-x}Ti_xO_{39-y}$.

2. Experimental

Polycrystalline samples of $Nd_{18}Li_8Co_{4-x}Fe_xO_{39-y}$ and $Nd_{18}Li_8Co_{4-x}Ti_xO_{39-y}$ were synthesised by grinding together stoichiometric quantities of the appropriate oxide starting materials (pre-dried neodymium(III) oxide (99.99%, Alfa Aesar), iron(III) oxide (99.99%, Alfa Aesar), cobalt(II, III) oxide (99.95%, Alfa Aesar), and titanium(IV) oxide (99.995%, Alfa Aesar)) and a 50% excess of volatile lithium carbonate (AnalaR) prior to firing in pellet form at 800 °C in air for 12 h. A further 50% excess lithium carbonate was ground into the reaction mixture before it was fired again in air for 1 h, as a pellet, at 1000 °C. X-ray powder diffraction was used to monitor the progress of the reactions. Further one-hour firings, with the addition of 50% excess lithium carbonate, were carried out on samples that X-ray powder diffraction showed to be impure at this stage.

All X-ray powder diffraction was carried out on a Philips X'pert diffractometer operating with Cu $K\alpha_1$ radiation with a step size of $\Delta 2\theta = 0.0084^\circ$. High-intensity X-ray powder diffraction data were collected over a small angular range ($15 \le 2\theta/^\circ \le 40$) in an attempt to detect impurities. High-resolution X-ray powder diffraction data for use in quantitative analysis were collected over the angular range $5 \le 2\theta/^\circ \le 125$. The X-ray scattering from these materials is dominated by the heavy metals and consequently it was not possible to perform a full structural analysis using these data. Limited Rietveld [7] refinements were carried out using the GSAS [8] suite of programs in order to determine the unit-cell parameters. Backgrounds were fitted using a Chebyshev polynomial of the first kind and the peak shape was modelled using a pseudo-Voigt function.

The diffractometer D2b at the Institut Laue Langevin, Grenoble, France was used to collect neutron powder diffraction data on selected samples using a wavelength of ~1.59 Å. The unit-cell parameters derived from X-ray diffraction data were used to calibrate accurately the neutron wavelength. Data were collected over the angular range $5 \le 2\theta/^\circ \le 160$ with a step size $\Delta 2\theta = 0.05^\circ$ at room temperature. Samples (~0.5 g) were contained within vanadium cans (ϕ=5 mm). Rietveld refinements of the structures were carried out using the FULLPROF [9] programme. The background level was refined using the software. Peak shapes were modelled using a pseudo-Voigt function together with a correction for peak asymmetry at low angles.

Magnetic measurements were carried out on selected samples using a Quantum Design MPMS 5000 SQUID magnetometer. The magnetisation (M) was measured as a function of temperature on warming from 2 to 300 K after cooling both in zero field (ZFC) and in the measuring field of 100 Oe (FC). AC susceptibility data were recorded on one composition at 4 frequencies ($1 \le \omega/\mathrm{Hz} \le 1000$) in a direct field of ~2 Oe and an oscillating field of amplitude 3.5 Oe over an appropriate temperature range with ΔT=0.1 K.

The iron-57 Mössbauer spectrum of $Nd_{18}Li_8CoFe_3O_{39-y}$ was measured at 295 K with a constant-acceleration spectrometer, which utilised a rhodium-matrix cobalt-57 source and was calibrated at 295 K with α-iron powder. The Mössbauer spectral absorber contained 20 mg cm^{-2} of $Nd_{18}Li_8CoFe_3O_{39-y}$ powder mixed with boron nitride. The ideal thickness of the Mössbauer absorber is limited to this value because of the strong non-resonant scattering of the γ-rays by the eighteen neodymium ions per formula unit. This is, at least in part, responsible for the rather low signal to noise ratio observed.

3. Results

3.1. $Nd_{18}Li_8Co_{4-x}Fe_xO_{39-y}$

X-ray powder diffraction showed that single-phase products had been prepared for x=1, 2 and 3. In each case the diffraction pattern could be accounted for using a structural model based on $La_{18}Li_8Rh_5O_{39}$, which adopts space group $Pm\bar{3}n$. The unit cell parameter increased in a linear manner with increasing iron

content from $a=11.8658(1)$ Å when $x=1$ to 11.9266(2) Å when $x=3$.

Neutron diffraction data were collected from $Nd_{18}Li_8Co_3FeO_{39-y}$ and $Nd_{18}Li_8CoFe_3O_{39-y}$. Our analyses of these data took as a starting model the structure of $La_{18}Li_8Rh_5O_{39}$. The smaller and larger octahedral sites, labelled in the present case as Co1 and Co2, are the 2*a* and 8*e* sites, respectively. The smaller site, coloured green in Fig. 1(a), is coordinated by six O4 atoms, which would ideally occupy a 12*f* site but are actually disordered over a 25%-occupied 48l site, and the larger site, coloured red in Fig. 1(a), is coordinated by six O1 atoms on a crystallographically distinct 48*l* site. The disorder on the O4 site is thought to be a consequence of the need to lengthen the Co1–O4 bond in order to relax partially the coordination environment about the cation [1]. The trigonal prismatic site Li1, coloured blue in Fig. 1(a), is located on *x,x,x*, a 16*i* site, and is coordinated on one side by three O4 atoms and on the other by three O1 atoms. Atoms O2 and O3 do not interact strongly with the polyhedral chains; together with the Nd^{3+} ions they form the channels within which the chains lie, see Fig. 1(b). The short Nd1–O1, Nd2–O1 and Nd2–O4 distances within the structure provide links between the chains and the channels.

The initial stages of the refinement of the structure of $Nd_{18}Li_8Co_3FeO_{39-y}$ proceeded smoothly using this model, although an additional Li_2CO_3 impurity phase of less than 1 wt % was also detected in the neutron experiment. Refinement of the cation distribution over the two octahedral sites showed Co and Fe to be disordered over the 2*a* and 8*e* sites. This structural model then gave a good fit to the data, although a relatively large B_{iso} value was observed on the 16*i* trigonal-prismatic site occupied by Li. Refinement of the Li occupancy of the 16*i* trigonal-prismatic site did not significantly reduce the atomic displacement parameter and hence a stoichiometric composition was assumed. It has previously been reported [2–5] that in some compositions disorder between Li and the transition metals occupying the 8*e* octahedral site occurs. Structural models in which Fe and/or Co occupied the prismatic site with the displaced Li occupying the 8*e* (¼ ¼ ¼) octahedral site were therefore considered. The resultant structural models did not significantly improve the fit or reduce the B_{iso} value of the 16*i* trigonal-prismatic site. Hence the site was constrained to be fully occupied by Li with the Fe and Co cations disordered over the two octahedral sites. The displacement parameter at the O4 site was also unusually large and the occupation factor of this site was therefore allowed to vary. This resulted in a reduction in the value of both B_{iso} and χ^2. The composition refined to be $Nd_{18}Li_8Co_3FeO_{38.02(8)}$. The resulting structural parameters and bond lengths are listed in Tables 1 and 2, respectively, and the observed and calculated diffraction profiles are shown in Fig. 2. Analysis of the data collected on $Nd_{18}Li_8CoFe_3O_{39-y}$ proceeded in a similar manner, although in this case there was evidence for the presence of Fe on the 16*i* site and Li on the 8*e* site. In this case the composition refined to $Nd_{18}Li_8CoFe_3O_{37.75(9)}$. The structural parameters and bond lengths are included in Tables 1 and 2, respectively; the diffraction profiles are shown in Fig. S1.

The temperature dependence of the dc molar magnetic susceptibility of $Nd_{18}Li_8Co_{4-x}Fe_xO_{39-y}$ is shown in Fig. 3 for the compositions $x=1$ and 3. In both cases the inverse susceptibility is a linear function of temperature above 100 K. The parameters derived by fitting this region with a Curie–Weiss law are listed in Table 3. The susceptibility of the $x=1$ composition shows hysteresis between the FC and ZFC data below ~14 K, and a maximum is apparent in both data sets at 2.3(1) K. The behaviour of the composition $x=3$ is very different. Hysteresis is observed below ~12 K and the ZFC susceptibility passes through a maximum at 4.3(3) K. The temperature gradient of the FC susceptibility changes at this temperature, but no maximum is observed. The ac susceptibility of the composition $x=3$ is shown in Fig. 4. The temperature of the transition in the real part of the susceptibility is clearly frequency-dependent. This dependence can be parameterized as the ratio of the relative change in the transition

Table 1
Structural parameters of $Nd_{18}Li_8Co_3FeO_{38.02}$ and $Nd_{18}Li_8CoFe_3O_{37.75}$ at room temperature in space group $Pm\bar{3}n$.

		$Nd_{18}Li_8Co_3FeO_{38.02(8)}$	$Nd_{18}Li_8CoFe_3O_{37.75(9)}$
a (Å)		11.8658	11.9266
R_{wp}		0.0349	0.0323
χ^2		1.67	1.62
Nd1 24*k*	*y*	0.3069(3)	0.3071(3)
0 *y z*	*z*	0.3030(3)	0.3045(3)
	B_{iso} (Å^2)	0.34(4)	0.53(4)
Nd2 12*f*	*x*	0.3476(2)	0.3485(3)
x 0 0	B_{iso} (Å^2)	0.12(5)	0.14(6)
Co1(Fe) 2*a*	B_{iso} (Å^2)	0.9(2)	0.7(2)
0 0 0	Co occupancy[a]	0.25(3)	0.13(3)
	Fe occupancy	0.75(3)	0.87(3)
Co2(Fe/Li) 8*e*	B_{iso} (Å^2)	2.0(3)	0.9(2)
¼ ¼ ¼	Co occupancy[a]	0.688(8)	0.22(1)
	Fe occupancy	0.063(8)	0.45(1)
	Li occupancy	0	0.09(1)
Li1(Fe) 16*i*	*x*	0.3708(8)	0.3685(8)
x x x	B_{iso} (Å^2)	2.6(3)	0.9(4)
	Li occupancy[a]	1	0.958(5)
	Fe occupancy	0	0.042(5)
O1 48*l*	*x*	0.8628(3)	0.8643(3)
x y z	*y*	0.8593(3)	0.8595(3)
	z	0.6956(2)	0.6942(2)
	B_{iso} (Å^2)	0.62(3)	0.79(4)
O2 6*d*	B_{iso} (Å^2)	0.6(1)	0.9(1)
¼ ½ 0			
O3 12*g*	*x*	0.6326(5)	0.6313(5)
x 0 ½	B_{iso} (Å^2)	0.80(9)	0.88(10)
O4 48*l*	*x*	0.1507(7)	0.1517(8)
x y z	*y*	0.016(2)	0.021(2)
	z	0.018(2)	0.018(2)
	B_{iso} (Å^2)	1.5(3)	0.9(3)
	occupancy[a]	0.209(3)	0.198(3)

[a] Fractional occupancy.

Table 2
Bond lengths (Å) and bond angles (deg.) in $Nd_{18}Li_8Co_3FeO_{38.02}$ and $Nd_{18}Li_8CoFe_3O_{37.75}$ at room temperature.

	$Nd_{18}Li_8Co_3FeO_{38.02}$	$Nd_{18}Li_8CoFe_3O_{37.75}$
Nd1–O1	2.580(4) × 2	2.619(4) × 2
	2.557(4) × 2	2.563(5) × 2
	2.505(2) × 2	2.503(4) × 2
Nd1–O2	2.433(4)	2.429(4)
Nd1–O3	2.415(4)	2.425(4)
	3.056(4)	3.092(4)
Nd2––O1	2.387(3) × 4	2.385(3) × 4
Nd2–O3	2.397(5) × 2	2.391(5) × 2
Nd2–O4	2.354(9)[a]	2.370(11)[a]
Co1(Fe)–O4	1.811(9)[a] × 6	1.839(10)[a] × 6
Co2(Fe/Li)–O1	1.972(3) × 6	2.002(3) × 6
Li1(Fe)–O1	2.085(10) × 3	2.082(10) × 3
Li1(Fe)–O4	2.19(2)[a] × 3	2.24(2)[a] × 3
Li1(Fe)–Li1(Fe)	3.068(13)	3.137(13)
Co1(Fe)–Li1	2.657(9)	2.716(10)
Co2(Fe/Li)–Li1	2.481(9)	2.448(10)
Nd1–Nd1 (pore size)	6.213(1)	6.253(1)
O1–Co2(Fe/Li)–O1	89.3(2)	88.4(2)
	89.5(2)	89.9(2)
	91.7(2)	91.7(2)

[a] Average bond length to a disordered oxygen site.

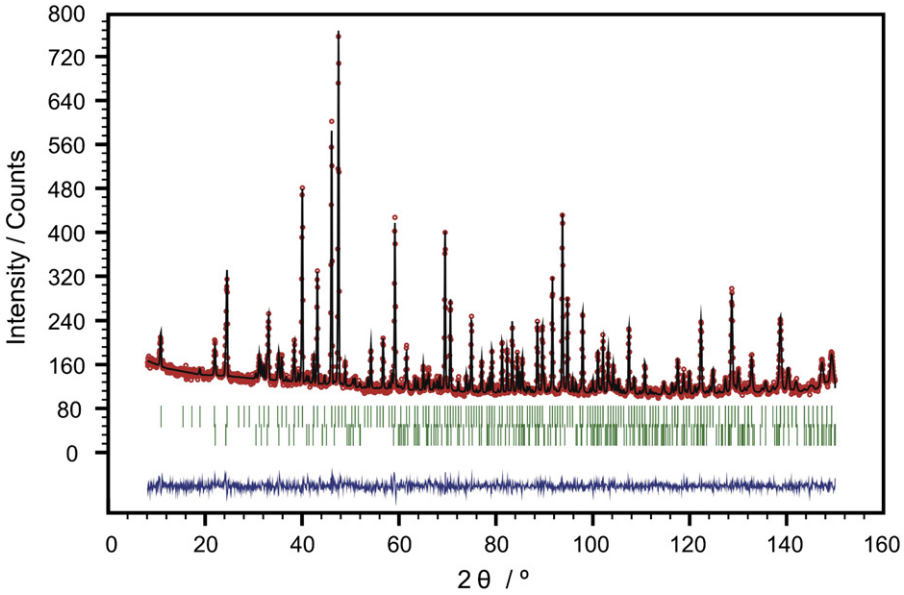

Fig. 2. Observed and calculated neutron diffraction profiles for $Nd_{18}Li_8Co_3FeO_{38.02}$; a difference curve is shown below. The upper and lower sets of vertical bars mark the positions of reflections attributable to the principal phase and Li_2CO_3, respectively.

temperature to the decadic shift in frequency, $\Delta T_f/T_f\Delta\log\omega$ [10], which takes a value of 0.049. The imaginary component of the susceptibility, χ'', is non-zero below ~6 K and a maximum is also observed close to the transition temperature and for all frequencies; the minimum in $d\chi''/dT$ is co-incident with the maximum value of χ'.

The iron-57 Mössbauer spectrum of $Nd_{18}Li_8CoFe_3O_{37.75}$ measured at 295 K is shown in Fig. 5. The spectrum indicates that $Nd_{18}Li_8CoFe_3O_{37.75}$ is paramagnetic at this temperature. It has been fitted with three doublets assigned to the 2*a*, 8*e* and 16*i* sites, respectively; the relative areas of these sites have been constrained to 29.4%, 59.12% and 11.48%, respectively, the fractional iron content of these crystallographic sites as determined at room temperature by powder neutron diffraction, see Table 1. The linewidth was constrained to be the same for each site; it refined to a value of 0.34(1) mm s^{-1}. The resulting fit, see Fig. 5, and the corresponding spectral parameters, see Table 4, suggest that $Nd_{18}Li_8CoFe_3O_{37.75}$ formally contains high-spin Fe^{3+} cations on the 8*e* and 16*i* sites and low-spin Fe^{4+} cations on the 2*a* site. The constraint based on the relative areas of the three components has been applied because the lack of detail in the paramagnetic Mössbauer spectrum renders several fitting models perfectly satisfactory from the statistical and physical points of view and because a reasonable analysis of the Mössbauer spectrum must include all available information and specifically the neutron diffraction results.

3.2. $Nd_{18}Li_8Co_{4-x}Ti_xO_{39-y}$

X-ray powder diffraction showed that a single-phase compound could only be prepared for the $x=1$ composition, $Nd_{18}Li_8Co_3TiO_{39-y}$. Analysis of the neutron diffraction data proceeded smoothly using the structural model described above. Cobalt and titanium were found to be disordered over the 2*a* and 8*e* sites, but there was no evidence for the presence of transition-metal cations on the 16*i* sites. The disordered arrangement of cobalt, an element with a positive scattering length, and titanium, an element with a negative scattering length, results in small mean scattering lengths at the 2*a* and 8*e* octahedral sites. It was therefore necessary to constrain the displacement parameters, B_{iso}, at these two sites to an arbitrary value, chosen to be zero. Refinements in which they were constrained to a value of 0.5 $Å^2$ resulted in occupancy factors that differed by <0.01 from those reported in Table 5. In contrast to the iron-containing compositions described above, the O4 site in the titanium-containing composition could be modelled by displacing the anion along only one axis, that is by locating it on a half-occupied 24*k* site rather than on a quarter-occupied 48*l* site. However, our initial refinements again resulted in a displacement parameter at the O4 site that was large enough to suggest that the site is only partially occupied, and subsequent refinements showed the composition to be $Nd_{18}Li_8Co_3TiO_{38.06(8)}$. The structural parameters and bond lengths are listed in Tables 5 and 6, respectively. The observed and calculated neutron diffraction profiles are shown in Fig. S2.

The temperature dependence of the dc molar susceptibility of $Nd_{18}Li_8Co_3TiO_{38.06(8)}$ is shown in Fig. 6. Fitting the data collected above 165 K to the Curie–Weiss law resulted in values of 32.00(6) cm^3 K mol^{-1} and −50.8(5) K for the Curie constant and the Weiss temperature, respectively. No hysteresis is observed throughout the measured temperature range and the susceptibility reaches a maximum value at 2.2(1) K.

4. Discussion

4.1. $Nd_{18}Li_8Co_{4-x}Fe_xO_{39-y}$

Although we have been unable to prepare the cobalt-free $x=4$ composition, the results presented above show that this crystal structure can tolerate vacancies on the 8*e* site when elements other than cobalt are present. As expected, the unit-cell parameter increases as cobalt is replaced by iron and the bond lengths in the Nd–O framework are unremarkable. The ability of the *Ln* cation to control the cation content of the polyhedral chains can be understood by comparing the width of the hexagonal cavity in this compound, described as the pore size in Table 2, with those of 6.397(1) and 6.321(3) Å found [4,5] in La- and Pr-based analogues, respectively. However, our data demonstrate that the system is not a simple solid solution. Our previous study [2] of the $x=0$ composition concluded that the anion sublattice was fully occupied, and hence that only Co^{4+} was present. In contrast,

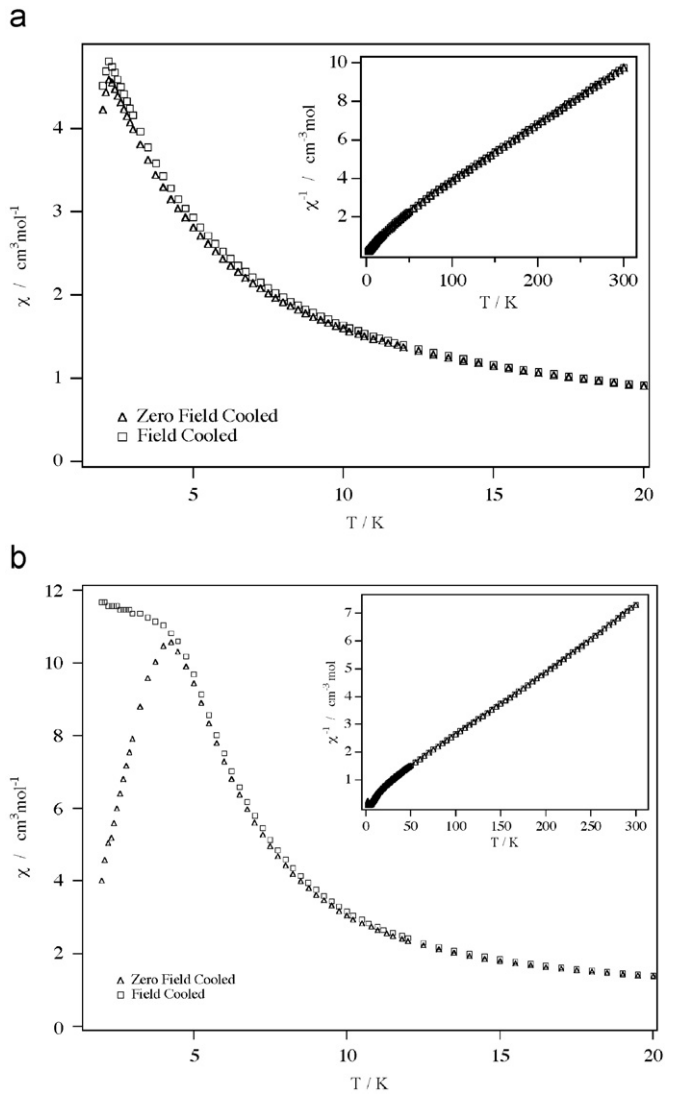

Fig. 3. Temperature dependence of the dc molar magnetic susceptibility of (a) $Nd_{18}Li_8Co_3FeO_{38.02}$ and (b) $Nd_{18}Li_8CoFe_3O_{37.75}$. The insets show the temperature dependence of the inverse susceptibility.

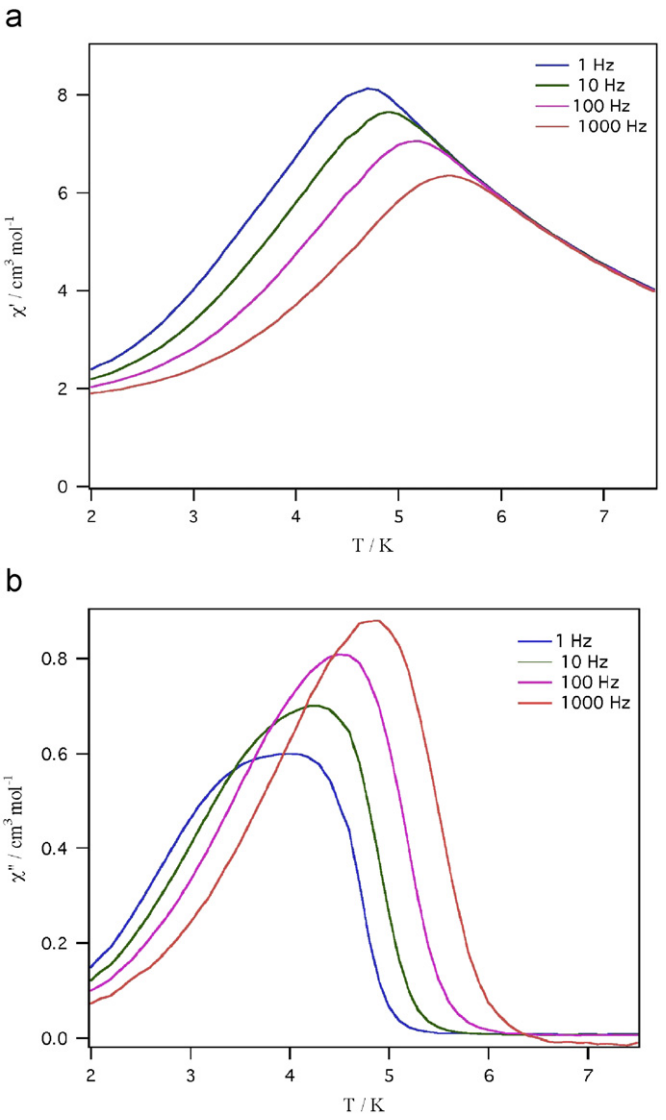

Fig. 4. Temperature and frequency dependence of the (a) real and (b) imaginary components of the ac molar susceptibility of $Nd_{18}Li_8CoFe_3O_{37.75}$.

Table 3
Curie–Weiss parameters of $Nd_{18}Li_8Co_{4-x}Fe_xO_{39-y}$.

x	C (cm^3 K mol^{-1})	θ (K)
1	34.06(4)	−31.9(3)
3	43.9(1)	−15.2(5)

in the case of $Nd_{18}Li_8Co_3FeO_{38.02}$ and $Nd_{18}Li_8CoFe_3O_{37.75}$, described in Table 1, there is evidence of vacant sites on the O4 sublattice: the presence of these vacancies requires the presence of trivalent cations somewhere in the structure. The 2*a* site is occupied by both cobalt and iron, albeit with a disproportionately high concentration of the latter. The short metal–oxygen distance around this site leads us to conclude that, as in the majority of the isostructural compounds studied to date, these cations are in a low-spin, tetravalent state. The Co1(Fe)–O4 bond length of 1.811 Å in $Nd_{18}Li_8Co_3FeO_{38.02}$ is the same as that measured in $Nd_{18}Li_8Co_4O_{39}$ and smaller [2] than that of 1.855 Å in $Nd_{18}Li_8Fe_5O_{39}$. The increased length, 1.839 Å, of the corresponding bond in $Nd_{18}Li_8CoFe_3O_{37.75}$ reflects the increased concentration of Fe^{4+}, but is still less than the distance observed in $Nd_{18}Li_8Fe_5O_{39}$.

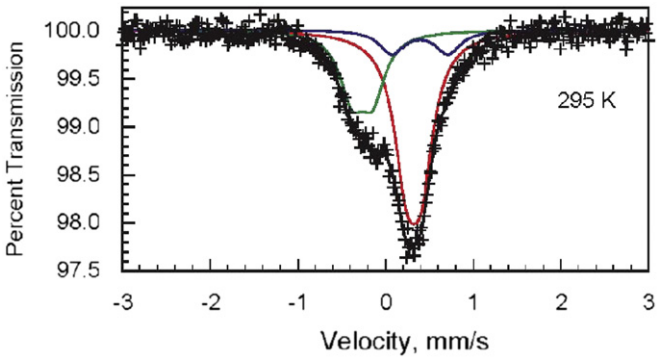

Fig. 5. Iron-57 Mössbauer spectrum of $Nd_{18}Li_8CoFe_3O_{37.75}$ obtained at 295 K. The components assigned to the 2*a*, 8*e* and 16*i* sites are indicated in green, red and blue, respectively; this colour scheme matches that used in Fig. 1. (For interpretation of the references to color in this figure legend, the reader is referred to the web version of this article.)

The presence of vacancies on the O4 site lowers the coordination number of the 2*a* sites and thus facilitates the accommodation of the larger Fe^{4+} cation. It is interesting to note that the isotropic

Table 4
Mössbauer Spectral Parameters for $Nd_{18}Li_8CoFe_3O_{37.75}$ at 295 K.

Iron site	δ (mm/s)[a]	ΔE_Q (mm/s)	Γ (mm/s)	Area (%)
2*a*	−0.264(6)	0.23(1)	0.34(1)	29.40[b]
8*e*	0.323(3)	0.17(1)	0.34(1)	59.12[b]
16*i*	0.394(2)	0.64(3)	0.34(1)	11.48[b]

[a] Isomer shifts are given relative to 295 K α-iron powder.
[b] Parameter constrained to the value given.

Table 5
Structural parameters of $Nd_{18}Li_8Co_3TiO_{38.06}$ at room temperature in space group $Pm\bar{3}n$.

a (Å)		11.86892(9)
R_{wp}		0.0325
χ^2		1.91
Nd1 24*k*	*y*	0.3058(3)
0 y z	*z*	0.3030(3)
	B_{iso} (Å^2)	0.42(4)
Nd2 12*f*	*x*	0.3492(3)
x 0 0	B_{iso} (Å^2)	0.22(5)
Co1(Ti) 2*a*	B_{iso} (Å^2)	0.0
0 0 0	Co occupancy[a]	0.64(2)
	Ti occupancy	0.36(2)
Co2(Ti) 8*e*	B_{iso} (Å^2)	0.0
¼ ¼ ¼	Co occupancy[a]	0.590(5)
	Ti occupancy	0.160(5)
Li1 16*i*	*x*	0.3634(8)
x x x	B_{iso} (Å^2)	1.8(3)
O1 48*l*	*x*	0.8640(3)
x y z	*y*	0.8591(3)
	z	0.6953(2)
	B_{iso} (Å^2)	0.80(4)
O2 6*d*	B_{iso} (Å^2)	1.0(2)
¼ ½ 0		
O3 12*g*	*x*	0.6323(5)
x 0 ½	B_{iso} (Å^2)	0.8(1)
O4 24*k*	*y*	0.028(1)
0 *y z*	*z*	0.152(1)
	B_{iso} (Å^2)	2.6(4)
	Occupancy[a]	0.422(6)

[a] Fractional occupancy.

Table 6
Bond lengths (Å) and bond angles (deg.) in $Nd_{18}Li_8Co_3TiO_{38.06}$ at room temperature.

Nd1–O1	2.593(4) × 2
	2.537(5) × 2
	2.509(4) × 2
Nd1–O2	2.430(4)
Nd1–O3	2.429(4)
	3.069(4)
Nd2–O1	2.384(4) × 4
Nd2–O3	2.381(5) × 2
Nd2–O4	2.364(12)[a]
Co1(Ti)–O4	1.834(12)[a] × 6
Co2(Ti)–O1	1.982(4) × 6
Li1–O1	1.996(10) × 3
Li1–O4	2.31(2)[a] × 3
Li1–Li1	3.243(13)
Co1(Ti)–Li1	2.808(9)
Co2(Ti)–Li1	2.331(9)
Nd1–Nd1 (pore size)	6.209(1)
O1–Co2(Ti)–O1	88.8(3)
	89.5(3)
	92.2(3)

[a] Average bond length to a disordered oxygen site.

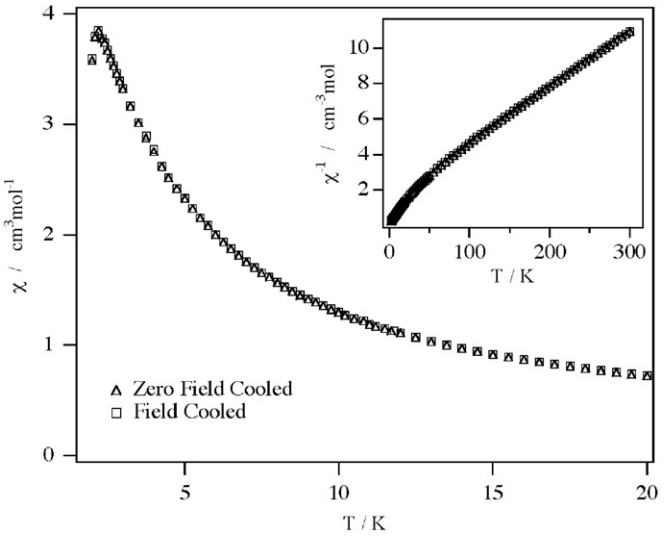

Fig. 6. Temperature dependence of the dc molar magnetic susceptibility of $Nd_{18}Li_8Co_3TiO_{38.06}$. The insets show the temperature dependence of the inverse susceptibility.

displacement parameter associated with the 2*a* site is larger in $Nd_{18}Li_8Co_3FeO_{38.02}$ than in comparable compositions in which the site is six-coordinate [2,3]. This can be interpreted as being a consequence of a reduction in the chemical pressure which we have previously argued exists within this structure. We also note that the Fe:Co ratio in $Nd_{18}Li_8CoFe_4O_{39}$ is sufficient to exclude cobalt from the 2*a* site [3], whereas the lower ratio in $Nd_{18}Li_8CoFe_3O_{37.75}$ is not.

The refined composition of $Nd_{18}Li_8Co_3FeO_{38.02}$ requires a mean oxidation state of 3.33 for the cobalt and iron cations on the 8*e* sites, that is one third of the filled sites are occupied by a tetravalent cation. Unfortunately, the low concentration of iron precluded the use of Mössbauer spectroscopy to determine the oxidation states of the two different elements in this sample. The mean Co2(Fe/Li)–O1 bond length of 1.972(3) Å around the 8*e* site is shorter than the Fe2–O1 distance of 2.028(3) Å in $Nd_{18}Li_8Fe_5O_{39}$ but longer than the Co2–O1 distance of 1.961(4) Å in $Nd_{18}Li_8Co_4O_{39}$. The relatively large isotropic displacement parameter of 2.0(3) Å^2 for the 8*e* site in $Nd_{18}Li_8Co_3FeO_{38.02}$ perhaps implies that the size of the octahedral 8*e* site is larger than is required by the smaller cation, which is consequently displaced, in a disordered manner, off the ideal site; we commented previously [2] that even in $Nd_{18}Li_8Co_4O_{39}$ the 8*e* site was larger than was needed to accommodate a low-spin Co^{4+} cation. The Curie constant of 34.06(4) cm^3 K mol^{-1} determined for $Nd_{18}Li_8Co_3FeO_{38.02}$ is slightly greater than that of 32.13(5) cm^3 K^{-1} mol^{-1} reported for $Nd_{18}Li_8Co_4O_{39}$ but the number of possible combinations of high-spin and low-spin cations in different oxidation states, together with an enforced but inappropriate reliance on the spin-only formula, makes the assignment of oxidation states and spin states in $Nd_{18}Li_8Co_3FeO_{38.02}$ difficult. However, the increase in the Curie constant suggests that some of the iron must enter the structure as high-spin Fe^{3+}, presumably on the expanded 8*e* site. It is unusual not to observe some Li^+ cations on the 8*e* site in this structure, but their absence in the present case can be attributed to the relatively small size of the 8*e* site. This is consistent with the structure of $Nd_{18}Li_8Co_4O_{39}$, where the 8*e* site is also too small to accommodate the alkali–metal cation. The relatively large value, 2.6 Å^2, of the isotropic displacement parameter at the 16*i* site in $Nd_{18}Li_8Co_3FeO_{38.02}$ might reflect cation displacements which themselves occur as a consequence of the partial occupancy of the O4 site.

The anion deficiency in $Nd_{18}Li_8CoFe_3O_{37.75}$ is somewhat higher than that found in $Nd_{18}Li_8Co_3FeO_{38.02}$, and the average oxidation state of the *d*-block cations not on the 2*a* site is reduced to 3.16. The Co2(Fe/Li)–O1 bond length around the 8*e* site is increased to 2.002(3) Å, closer to the value of 2.028(3) Å found [2] in $Nd_{18}Li_8Fe_5O_{39}$. The increase in size of the octahedral 8*e* site is sufficient to allow some of the Li^+ cations to occupy the 8*e* sites instead of being confined to the prismatic 16*i* site as in $Nd_{18}Li_8Co_4O_{39}$ and $Nd_{18}Li_8Co_3FeO_{38.02}$. Surprisingly, the introduction of cation disorder on the 16*i* site is accompanied by a decrease in the displacement parameter at this site. The higher concentration of iron in $Nd_{18}Li_8CoFe_3O_{37.75}$ made feasible a study by Mössbauer spectroscopy. The relative areas of the spectral components, see Fig. 5, agree with the cation distribution determined from the neutron diffraction data; the fitted parameters in Table 4 confirm that the 2*a* site is occupied by Fe^{4+} and the 8*e* and 16*i* sites by high-spin Fe^{3+}. If we assume that all the cobalt cations on the 8*e* site are present as Co^{4+} we calculate a mean oxidation state of 3.29 for the *d*-block cations distributed over the 8*e* and 16*i* sites. This is higher than the value calculated from the composition, but reasonable when the error in the latter is taken into account. Furthermore, if we assume that the increased size of the coordination octahedron around the 8*e* site allows Co^{4+} to adopt a high-spin state, then the calculated Curie constant of 43.4 $cm^3\,K\,mol^{-1}$ is in excellent agreement with that of 43.9(1) $cm^3\,K\,mol^{-1}$ determined for $Nd_{18}Li_8CoFe_3O_{37.75}$ from the experimental data; a value of 39.9 $cm^3\,K\,mol^{-1}$ is obtained if Co^{4+} is assumed to be in a low-spin state on the 8*e* site. We note that the presence of only high-spin $3d^5$ cations on the 8*e* and 16*i* sites increases the value of predictions based on the spin-only formula.

The magnitude of the magnetic susceptibility of the composition $Nd_{18}Li_8Co_3FeO_{38.02}$ is slightly larger than that reported previously [2] for $Nd_{18}Li_8Co_4O_{39}$, as is to be expected if low-spin Co^{4+} is replaced in part by high-spin Fe^{3+}. The hysteresis between the ZFC and FC susceptibilities is apparent at a slightly higher temperature in $Nd_{18}Li_8Co_3FeO_{38.02}$, which is also consistent with a higher spin concentration. However, the susceptibility maximum occurs at the same temperature in the two compositions, an observation that supports our previous proposal that this maximum marks the onset of antiferromagnetic ordering on the neodymium sublattices.

The temperature dependence of the magnetic susceptibility of $Nd_{18}Li_8CoFe_3O_{37.75}$ is very different from that of $Nd_{18}Li_8Co_3FeO_{38.02}$ and bears a closer resemblance [2] to that of $Nd_{18}Li_8Fe_5O_{39}$. As was the case for the latter compound, the clear hysteresis present below the temperature of the susceptibility maximum suggests the formation of a spin-glass phase. The frequency dependence of the transition temperature and the appearance of an imaginary component in the ac susceptibility, see Fig. 4, are consistent with this interpretation, and the value of $\Delta T_f/T_f\Delta\log\omega$ determined from the data is typical of an insulating spin glass [10]. The existence of a maximum in the ZFC susceptibility, rather than simply a change of slope, shows that the strongly-paramagnetic Nd^{3+} cations must be involved in the spin-freezing process. This is consistent with previous studies, which have found that spin-glass formation occurs when *Ln* is paramagnetic and there is a high concentration of unpaired electrons on the 8*e* sites. On the basis of these studies, it was concluded [5] that the *Ln* cation plays an important role in the inter-cation interactions in these compounds. The present study shows that this conclusion is true even when a quarter of the 8*e* sites are unoccupied; the magnetic behaviour is sensitive to the magnitude of the magnetic moment of the transition-metal cations, but relatively insensitive to the presence of vacancies on that sublattice.

4.2. $Nd_{18}Li_8Co_{4-x}Ti_xO_{39-y}$

$Nd_{18}Li_8Co_4O_{39}$ can only accommodate a relatively low level of titanium substitution, perhaps because of the larger size of titanium cations compared to those of cobalt and iron. As expected, the unit cell increases in size when titanium is introduced into the structure, although the diameter of the hexagonal cavity containing the polyhedral chains remains comparable to that in the Fe/Co compositions discussed above. The size of the coordination octahedron around the 8*e* site is intermediate between those listed in Table 2 for the iron-substituted compositions, but is apparently too small to permit lithium cations to occupy the 8*e* site. The mean Co1(Ti)–O4 bond length of 1.834(12) Å around the 2*a* site is longer than those in $Nd_{18}Li_8Co_4O_{39}$ and $Nd_{18}Li_8Co_3FeO_{38.02}$, as is to be expected in view of the relatively large size of the titanium cation. However, the site is too small to accommodate a six-coordinate Ti^{4+} cation, and the location of titanium cations on this site is probably only made possible by the reduction in the coordination number brought about by the presence of vacancies on the O4 site. In the case of $La_{18}Li_8Rh_4TiO_{39}$ the 2*a* site is 64% occupied by Ti^{4+}, but the presence of the larger La^{3+} cation resulted in a mean bond length of 1.924 Å and no anion deficiency was detected [6].

The presence of vacant anion sites in $Nd_{18}Li_8Co_3TiO_{38.06}$ necessitates the presence of trivalent *d*-block cations in the structure. The chemistry of the two elements leads us to expect that Co^{4+} would be reduced more readily than Ti^{4+}, and that the oxygen deficiency is accommodated by the cation combination $2Co^{3+}+Co^{4+}+Ti^{4+}$. We assume that the small 2*a* site is occupied by a mixture of low-spin Co^{4+} and Ti^{4+}, leaving the larger trivalent cations and the remaining tetravalent cations to occupy the 8*e* site. If Co^{3+} is also in the low-spin state, the predicted Curie constant, assuming a spin-only contribution from low-spin Co^{4+} and that Nd^{3+} behaves as an ideal $^4I_{9/2}$ cation, is 29.86 $cm^3\,K\,mol^{-1}$, slightly less than the observed value of 32.00(6) $cm^3\,K\,mol^{-1}$. Better agreement between the observed and calculated (31.3 $cm^3\,K\,mol^{-1}$) Curie constants is achieved if we assume that the Co^{4+} cations on the 8*e* site adopt a high-spin configuration. The mean bond length around this site is intermediate between those measured in the two iron-containing compositions described above, and this model is therefore plausible. However, we should emphasise that this level of interpretation relies on Nd^{3+} behaving as an ideal $^4I_{9/2}$ cation in our compounds. The magnetic susceptibility of $Nd_{18}Li_8Co_3TiO_{38.06}$ shows none of the hysteresis observed in $Nd_{18}Li_8Co_4O_{39}$, $Nd_{18}Li_8Co_3FeO_{38.02}$ or $Nd_{18}Li_8CoFe_3O_{37.75}$. It seems likely that the combination of diamagnetic Ti^{4+} and cation vacancies reduce the involvement of the 8*e* site in the magnetic interactions to such an extent that the antiferromagnetic superexchange between Nd^{3+} cations is the only significant magnetic coupling in $Nd_{18}Li_8Co_3TiO_{38.06}$, and that this compound consequently adopts an antiferromagnetic ground state below $T_N=2.2$ K.

5. Conclusions

The crystal structure adopted by the compounds described above permits a remarkable flexibility in composition. Our previous work [1–6] has suggested that cations can adopt unusual oxidation states and spin states as a consequence of the chemical pressure applied on the polyhedral chains by the *Ln*–O framework. The results presented herein extend the scope of our earlier studies to include further cation-deficient compositions. In contrast to the case of $Nd_{18}Li_8Co_4O_{39}$, the first such composition to be reported, the cation deficiency in the newly-synthesised compounds is partially compensated by the formation of oxide

vacancies. The three compositions discussed all show different magnetic behaviour at low temperatures, and thus illustrate the range of complexity that can occur in the electronic properties of this structural family. The temperature dependence of the susceptibility of $Nd_{18}Li_8Co_3TiO_{38.06}$ can be accounted for by assuming that long-range antiferromagnetic ordering occurs on the neodymium sublattices below 2.2 K. The increased concentration of magnetic cations on the 8*e* site in $Nd_{18}Li_8Co_3FeO_{38.02}$ leads to some hysteresis as the Nd^{3+}–8*e*-cation interactions become significant above 2.2 K and in $Nd_{18}Li_8CoFe_3O_{37.75}$ these interactions compete sufficiently strongly with those between Nd^{3+} cations that a spin-glass state is formed; the behaviour of the latter composition is qualitatively similar to that of the $Nd_{18}Li_8Co_xFe_{5-x}O_{39}$ system described previously [3]. The central role of the lanthanide cations in this progression of the magnetic properties is consistent with the behaviour of the $Ln_{18}Li_8Rh_{5-x}Fe_xO_{39}$ compositions reported previously [5] and it appears that the properties are more sensitive to the magnetic nature of the lanthanide cation than they are to the presence of vacancies on the transition-metal sublattice.

Acknowledgments

We are grateful to Dr. C. Ritter for providing experimental assistance at the ILL in Grenoble, France. F.G. acknowledges the financial support of the Fonds National de la Recherche Scientifique, grants 9.456595 and 1.5.064.05. N.T. was supported by a Royal Thai Government Scholarship and S.W. by a Nuffield Undergraduate-Research Bursary.

Appendix A. Supplementary materials

Supplementary materials associated with this article can be found in the online version at doi:10.1016/j.jssc.2011.07.020.

References

[1] P.P.C. Frampton, P.D. Battle, C. Ritter, Inorganic Chemistry 44 (2005) 7138.
[2] S.E. Dutton, P.D. Battle, F. Grandjean, G.J. Long, K. Oh-ishi, Inorganic Chemistry 47 (2008) 11212.
[3] S.E. Dutton, P.D. Battle, F. Grandjean, G.J. Long, P.A. van Daesdonk, Inorganic Chemistry 48 (2009) 1613.
[4] S.E. Dutton, P.D. Battle, F. Grandjean, G.J. Long, M.T. Sougrati, P.A. van Daesdonk, E. Winstone, Journal of Solid State Chemistry 182 (2009) 1638.
[5] P.D. Battle, S.E. Dutton, N. Thammajak, F. Grandjean, M.T. Sougrati, G.J. Long, K. Oh-ishi, S. Nakanishi, Inorganic Chemistry 49 (2010) 5912.
[6] P.D. Battle, S.E. Dutton, P.A. van Daesdonk, Journal of Solid State Chemistry. 183 (2010) 1620.
[7] H.M. Rietveld, Journal of Applied Crystallography 2 (1969) 65.
[8] A.C. Larson, R.B. von Dreele, General Structure Analysis System (GSAS) Los Alamos National Laboratories LAUR (1994) 86–748.
[9] J. Rodriguez-Carvajal, Physica B 192 (1993) 55.
[10] J.A. Mydosh, Spin glasses: an experimental introduction, Taylor & Francis, London, 1993.